Essential Readings in Light Metals: Cast Shop for Aluminum Production.
Edited by John F. Grandfield and Dmitry G. Eskin.

Light Metals — From *Light Metals 2001*, Joseph L. Anjier, Editor

Predicting Microstructure and Microsegregation in Multicomponent Aluminum Alloys

Xinyan Yan[1] Ling Ding[1] ShuangLin Chen[2] Fanyou Xie[1] M. Chu[3] Y. Austin Chang[1]

[1]University of Wisconsin-Madison, Department of Materials Science & Engineering
1509 University Avenue, Madison, Wisconsin 53706 USA

[2]CompuTherm,LLC, 437 S. Yellowstone Dr., Suite 217, Madison, WI53719, USA

[3]Alcoa Technical Center, Aluminum Company of America, Alcoa Center, PA 15069

Abstract

Accurate predictions of microstructure and microsegregation in metallic alloys are highly important for applications such as alloy design and process optimization. Restricted assumptions concerning the phase diagram could easily lead to erroneous predictions. The best approach is to couple microsegregation modeling with phase diagram computations. A newly developed numerical model for the prediction of microstructure and microsegregation in multicomponent alloys during dendritic solidification was introduced. The micromodel is directly coupled with phase diagram calculations using a user-friendly and robust phase diagram calculation engine-PANDAT. Solid state back diffusion, undercooling and coarsening effects are included in this model, and the experimentally measured cooling curves are used as the inputs to carry out the calculations. This model has been used to predict the microstructure and microsegregation in two multicomponent aluminum alloys, 2219 and 7050. The calculated values were confirmed using results obtained from directional solidification.
Keywords: Multicomponent Al alloys, microstructure, microsegregation, solidification, modeling, experiment.

1. Introduction

Microstructures are at the center of materials science and engineering. They are the strategic link between materials processing and materials behavior [1]. Microstructure control is therefore essential for any processing activity. Meanwhile, microsegregation phenomena are of technical importance since they have implications on the properties of the alloys. For example, the formation of brittle non-equilibrium phases can cause deterioration of the mechanical properties. Variations of concentration can produce inhomogeneous precipitations during subsequent heat treatment thus leading to poor fatigue resistance. Segregation can also cause other problems, such as corrosion resistance, etc. It is indeed that an accurate prediction of microsegregation and microstructure in metallic alloys is highly important.

Since the first analytical approach of Mehrabian and Flemings for a ternary alloy [2], numerous models based on phase diagrams have been developed for the simulation of microsegregation in multicomponent systems. The state of the art for the simulation methods has been summarized by Kraft and Chang[3]. The levels of complexity of micromodels vary considerably, but all require phase diagram information, i.e. the concentrations of the liquid and solid phase at the liquid/solid interface or the partition coefficients. However, the partition coefficient as a function of temperature and concentration of alloying elements is usually unknown for multicomponent systems. Some investigators often simplify the multicomponent systems to binary or ternary systems by neglecting some of the main components and all the minor alloy elements. Many simulation studies on multicomponent alloys often use linearized partition coefficients estimated from binary systems. These practices can lead to serious errors [4, 5]. The assumption of a constant partition coefficient is normally not a good one. Since nearly all commercial alloys are multicomponent in nature, there is an urgent industrial need to investigate and simulate more complex alloys. Also, the predictions of a micromodel are strongly affected by the shape of the local cooling curve [6]. At very high cooling rates, solute trapping [7, 8, 9] and other effects offset the local equilibrium at the interface, and undercooling phenomena need to be taken into account. Dendrite arm coarsening also contributes significantly to homogenization during solidification [10, 11]. In order to predict microstructure and microsegregation as a function of alloy chemistry and process variables, microscopic modeling should take into account all the thermodynamic and kinetic effects of the material system [11].

While a number of analytical and numerical studies of microsegregation of binary alloys have been reported [3,12], investigations of multicomponent alloys are rather limited. Kraft et al[11] developed an extensive micromodel considering all kinetic and thermodynamic effects. However, their model can be used only for ternary or quaternary alloys.

The objective of the present work is to develop a micro-model to predict the microstructure and microsegregation in multicomponent commerical cast alloys solidified at different cooling rates. To achieve this goal, this model was directly coupled with multicomponent phase diagram calculation, and different kinetic effects, such as non-equilibrium phase diagram due to solute trapping at high cooling rate, undercooling, solid back diffusion and dendrite arm coarsening, should be considered in the model. To verify this model, directional solidification experiments have performed for the 4-component Al-6.27Cu-0.22Si-0.19Mg wt% alloy (base of 2219 alloy) and the commercial 7 component 7050 alloys. These alloy systems were chosen because of their technological importance in the automobile and aerospace industries. In the following, we will present (1) a description of the micromodel and its coupling with phase diagram calculation, (2) the thermodynamic database, (3) the experimental method, (4) results and discussion, and finally conclusions.

2. Description of the Micro Model

The present numerical model predicts the secondary dendrite arm spacing, element distribution in the dendrite arms and types and amounts of non-equilibrium phases in the entire range of dendritic solidification in multicomponent alloys. The main thermodynamic and kinetic effects that can influence the solidification behavior are accounted for. The only major simplification of the model is that the geometry of the dendrites is assumed to be geometrically similar (plate, cylinder or sphere – like) throughout solidification.

This numerical micro-model is basically a modified Scheil model incorporating back diffusion, undercooling and dendrite arm coarsening. The most important extensions as compared to earlier models[3] are (I) extension to the higher order alloys, (II) direct coupling with multicomponent phase diagram calculation, (III) inclusion of undercooling effects and dendrite arm coarsening for multicomponent alloys and (IV) solid back diffusion during the whole solidification stage.

Since modeling of solidification relies heavily on information describing the solid-liquid interface and tie lines, incorrect assumptions concerning the phase diagram can easily lead to erroneous predictions. The best and most accurate method for treating the phase equilibrium at the interface is to couple the microsegregation modeling with phase diagram calculations[13]. Previously, this kind of coupling has been restricted to binary and ternary systems mainly due to a lack of a robust phase diagram calculation software and suitable interfaces[14, 3]. To this end, we have developed a micro-model which was directly coupled with phase diagram calculation for multi-component alloys. Very good agreement is obtained between the experimental data and the simulated results using the present method for multi-component aluminum alloys.

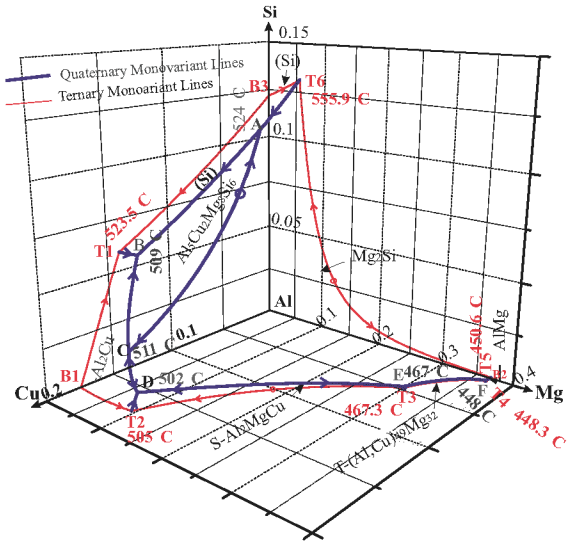

Figure 1. Calculated phase equilibria involving liquid and (Al) in Al-Cu-Mg-Si quaternary system(red lines are the three phase equilibria in ternary systems, blue lines are the four phase equilibria quaternary monovariant lines, points A, B, C, D, E and F are five-phase invariant points in quaternary system, points T1 to T6 are the four-phase invariant points in ternary systems, and points B1, B2 and B3 are the three-phase invariant points in binary systems)

To implement the phase equilibria calculation in the micromodeling, the multi-component phase diagram calculation interface-PANDAT[15] was used. This interface was developed by CompuTherm LLC. The important variables are transferred in this interface from one code segment to another. Using this interface, the tie lines in a multicomponent system can be calculated at each time step of the solidification process. Back diffusion in the solid, dendrite tip undercooling and dendrite arm coarsening are all considered in the micro-model. Back diffusion in the solid is obtained independently for each element by solving the Fick's second law numerically. Dendrite arm coarsening is calculated using the suggestion by Beaverstock [16], which takes into the consideration all solute elements for a multi-component system instead of only the element with the lowest value of coarsening parameter. Three geometric shapes, i.e. plate, cylinder and sphere, were used to describe the growing secondary or tertiary arms. In addition to the thermodynamic data inputs, cooling rate and physical properties, such as diffusion coefficients, surface tension, density and latent heat, are also needed. The results from the model-calculations are the types and amounts of phases present during and after solidification, the concentration distributions in the primary phase, liquid concentration and the dendrite arm spacings.

Table I Comparison of Calculated Invariant Equilibrium Temperatures with Experimental Data in the Al-Cu-Mg-Si System

Point	Reaction	Temp. (°C)	
		Exp.	Cal.
A	$L + Mg_2Si = (Al) + (Si) + Al_5Cu_2Mg_8Si_6$	521 [17] 529 [18]	524
C	$L+Mg_2Si=(Al)+\theta_{AlCu}+Al_5Cu_2Mg_8Si_6$	510 [19] 513 [20] 510 [17] 512 [21]	511
B	$L = (Al) + \theta_{AlCu} + (Si) + Al_5Cu_2Mg_8Si_6$	505 [17] 506.5 [19] 507 [21] 510 [20]	509
D	$L = (Al) + \theta_{AlCu} + Mg_2Si + S\text{-}CuMgAl_2$	500 [17] 507 [21] 500 [19]	502
E	$L + S = (Al) + Mg_2Si + T\text{-}CuMg_4Al_6$	464 [19] 467 [18]	467
F	$L = (Al) + \beta_{AlMg} + Mg_2Si + T\text{-}CuMg_4Al_6$	444 [17] 444~448 [18]	448

3. Aluminum Thermodynamic Database

As mentioned previously, a major obstacle to modeling multicomponent systems is the lack of phase diagram databases for these complex alloys. Recently, an advanced aluminum database with 12 components Al, Cu, Mg, Si, Fe, Mn, Zn, Ti, Ni, Cr, Zr and V has been developed[22]. All Al-containing ternary constituent systems and some important Al-containing quaternary systems, such as Al-Cu-Mg-Si[23], Al-Cu-Mg-Zn[24] and Al-Fe-Mg-Si et al., were assessed for this database. More than 210 different phases are contained in this database. The analytical

descriptions used are fully SGTE compatible. This database was used in present study.

The accuracy of phase diagram data is paramount in predicting microstructure and microsegregation. So, the reliability of the Al-database has been validated through a large amount of experimental data on multicomponent aluminum alloys[22, 23]. Consider the Al-Cu-Mg-Si quaternary system as an example. Figure 1 is a calculated liquidus projection of Al-Cu-Mg-Si system in Al-rich corner. As shown in this figure, there are six 5-phase invariant reactions (labeled as points A, B, C, D, E and F in the figure). All these 6 reactions have been reported and confirmed by different experimental investigations. As shown in Table I, the calculated temperatures of the invariant reactions and the compositions of the phases at the invariant temperatures are in good agreement with the experimental data. We believe that this database can be used to accurately predict the microstructure and microsegregation in aluminum alloys.

4. Experimental Method

a quaternary aluminum alloy, Al-6.27Cu-0.22Si-0.19Mg (wt%, base of A2219 alloy) and a 7050 commercial alloy were directionally solidified at a predetermined growth rate with thermal gradients kept at about 50 °C/cm near the solid/liquid interface. The thermal profiles within the sample during solidification were measured and recorded by an accurate temperature acquisition system (NI4300, National Instruments). The temperature profile recorded for each sample during solidification was used as the input for calculating the degree of microsegregation as presented later.

Each of the solidified samples was transversely cross-sectioned and polished but not etched. Composition measurements and microstructure analysis were carried out using a fully automated Cameca SX-50 Scanning Electron Microprobe. The composition measurements were carried out using a Wavelength Dispersive Spectrum method (WDS). Pure Al, Cu, Si, Mn, Fe, Zn and MgO were used as the standards. A total of 400 measurements were carried out automatically over an area of 800 X 800 μm^2. These measured data were analyzed and compared with the calculated values. Samples were metallographically examined to determine their SDAS using the image analysis system. The image analysis software--OPTIMAS 6.1 was used to measure the phase fractions.

5. Results and Discussion

5.1 Al-Cu-Mg-Si Alloy

5.1.1 Microstructures of Al-Cu-Mg-Si alloy

The quaternary Al-6.27Cu-0.22Si-0.19Mg alloy was solidified with solidification rates of 0.013, 0.05 and 0.15 mm/s under a temperature gradient of 50K/cm. The microstructures of the solidified samples are dendritic. A typical microstructure of the directionally solidified alloy is shown in Figure 2. In this BSE image, the dark areas are (Al) (aluminum phase) and the bright areas are θ (the Al_2Cu phases) and eutectics. The different gray scales show the varying contents of the solute in the primary (Al). The calculated fraction of solid vs. temperature relationships for this quaternary alloy solidified with a growth rate of 0.013 mm/s are shown in Figure 3. According to the Scheil model, the solidification sequence for this alloy is: L → (Al) → [L+ (Al) + θ](surface $T_1BCDT_2B_1T_1$ in Figure 1) → [L+ (Al) + θ + $Al_5Cu_2Mg_8Si_6$] (monovariant line CB in Figure 1) → [L + (Al) +

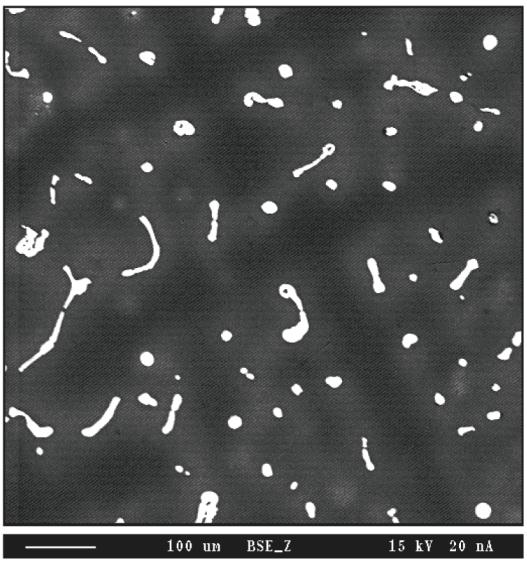

Figure 2 Typical dendrite structure in transverse section of the directionally solidified Al-6.27Cu-0.22Si-0.19Mg alloy at a growth rate of 0.05mm/sec with a temperature gradient of 50°C/cm at the liquid/solid interface

θ + $Al_5Cu_2Mg_8Si_6$ + (Si)](Invariant point B in Figure 1). Experimentally, there was no (Si) phase (or quaternary eutectics) formed according to metallographical examination and EPMA analysis, and even the $Al_5Cu_2Mg_8Si_6$ phases (or ternary eutectic) are very difficult to find in the microstructures. Only the result predicted by the modified Scheil model is in agreement with the experimental observation. The secondary dendrite arm spacings were measured metallographically at many locations. The average values of the measured spacings which had a maximum deviation of ±10 pct, are given in Table II. The second dendrite arm spacing decreases with increasing growth rate. Phase fractions obtained using a quantitative image analysis program are given in Table II. They were compared with the fractions of (Al) phase calculated from the modified Scheil, the Scheil and equilibrium conditions (lever rule). While the fractions of (Al) phase calculated from the Scheil model are less than the measured values and the fractions of (Al) calculated from lever rule are higher than the experimental results, those calculated

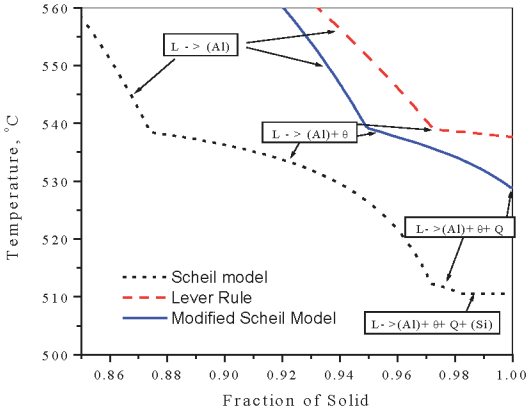

Figure 3 Fraction of solid vs. temperature for Al-6.27Cu-0.22Si-0.19Mg alloy calculated by Lever rule, the Scheil model and the modified Scheil model

from the modified model are in accord with the experimentally measured values. The calculated dendrite arm spacings are also in accord with the measured values.

Table II Comparison of experimental and calculated phase fractions and dendrite arm spacings

Growth Rate (mm/s)	λ_2,μm		Amount of Primary (Al), vol.%				
	Image Analysis	Model cal.	Area Scan	Image analysis	Model cal.	Scheil	Lever rule
0.013	130	132	95.8	94.7	94.1	87.4	97.3
0.05	74	72	95.8	95.3	95.0	87.4	97.3
0.15	62	63	96.0	95.4	95.7	87.4	97.3

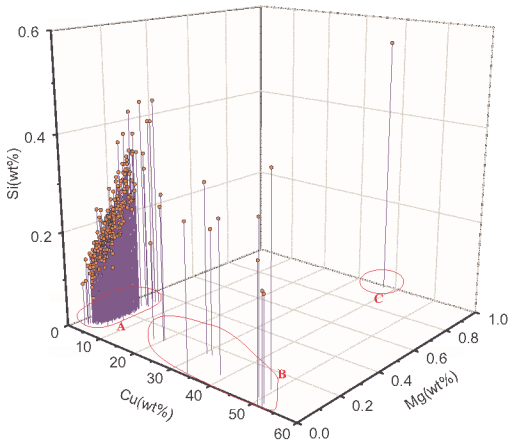

Figure 4. Experimental correlation between copper, silicon and magnesium content measured on Al-6.27Cu-0.22Si-0.19Mg alloy solidified at growth rate of 0.05 mm/sec/sec with temperature gradient of 50K/cm

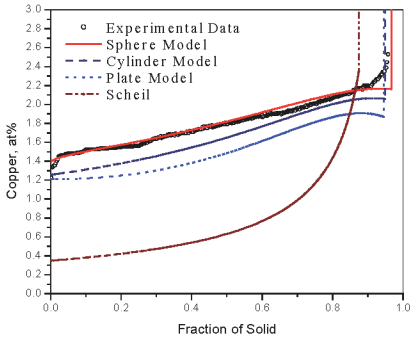

Figure 5. Cu concentration profiles in the primary dendrites as a function of the fraction of solid: comparison between the model-calculated values and experimental data for Al-6.27Cu-0.22Si-0.19Mg alloy solidified with a growth rate of 0.013 mm/s and a temperature gradient of 50°C/cm at the liquid /solid interface

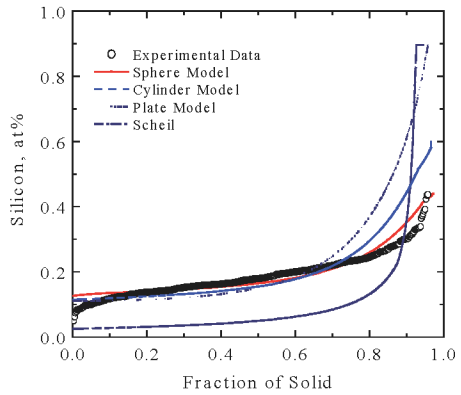

Figure 6. Si concentration profiles in the primary dendrites as a function of the fraction of solid: comparison between the model-calculated values and experimental data for Al-6.27Cu-0.22Si-0.19Mg alloy solidified with a growth rate of 0.013 mm/s and a temperature gradient of 50°C/cm at the liquid /solid interface

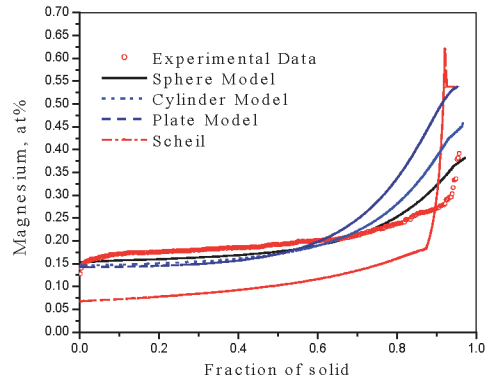

Figure 7. Mg concentration profiles in the primary dendrites as a function of the fraction of solid: comparison between the model-calculated values and experimental data for Al-6.27Cu-0.22Si-0.19Mg alloy solidified with a growth rate of 0.013 mm/s and a temperature gradient of 50°C/cm at the liquid /solid interface

5.1.2 Microsegregation in Al-Cu-Mg-Si Alloy

The area scan method noted previously was used to measure the microsegregation in the Al-6.27Cu-0.22Si-0.19Mg alloy solidified directionally at the three growth rates of 0.013, 0.05 and 0.15 mm/s. 400 measurements were made over an area of 800 X 800 μm^2 of each sample. We first discuss how to deal with these experimental data.

Figure 4 shows the measured 400 values of the copper content versus the corresponding values of the magnesium content and the silicon content in the sample solidified with growth rate of 0.015 mm/s. It is found that a large number of the points are distributed at low content in solutes (area A in Figure 4) and are

associated with measurements made on the primary (Al) phase. The remaining points with high Copper content (area B in Figure 4) correspond with the composition of θ phase, while the points with high magnesium content (points in area C of figure 4) are the composition of the $Al_5Cu_2Mg_8Si_6$ phase. No trace of (Si) was found. These points with high copper and magnesium contents are differentiated from those related to the primary phase. After this, the remaining data can be sorted in order to give a cumulative distribution of solution in the primary phase. Ordered integer numbers were assigned to the sorted points and the integer numbers were converted to volume fractions by dividing each data number by the total data number. The composition as a function of the volume fraction of solid was then plotted. The measured solute distribution of Cu, Mg and Si at a growth rate of 0.013 mm/s with a temperature gradient of 50K/cm are shown in Figures 5, 6 and 7 respectively.

Next, we compare the experimental measured concentration profiles with model-calculated results. Three dendrite arm geometries, plate, cylinder and sphere, were considered in the present micro-model. As shown in Figures 5-7, the calculated results were compared with those obtained under Scheil conditions and with the experimental data for the sample solidified at a growth rate of 0.013 mm/s with a temperature gradient of 50K/cm. Although the calculated values using the modified Scheil model improves irrespective of the geometries used to approximate the shapes of the dendrites, the spherical model yields values in best agreement with the experimental data. Good agreement was also obtained for samples solidified with growth rates of 0.05 and 0.15 mm/s.

It is evident that the Scheil model does not give a good description of the experimental data (phase fractions and solute concentration gradients).The modified micro-model, which considers all the kinetic effects and is directly coupled with the multicomponent phase diagram computation, can predict the microstructure and microsegregation in Al-Cu-Mg-Si quaternary alloys accurately.

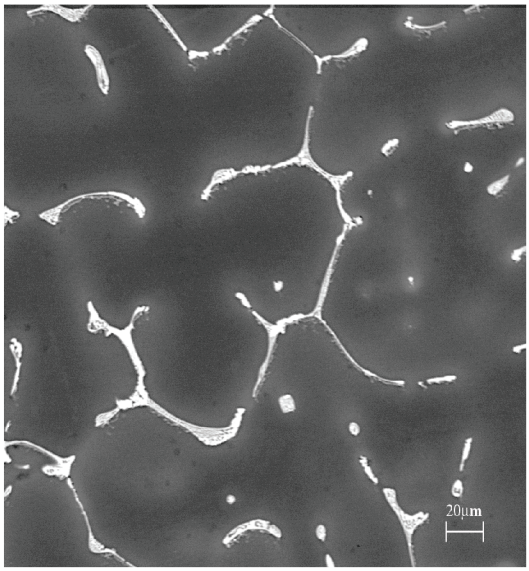

Figure 8. Typical microstructure in transverse section of the directionally solidified 7050 alloy at growth rate of 0.1 mm/sec with a temperature gradient of 50°C/cm at the liquid/solid interface

5.2 7050 Commercial Alloy

5.2.1 Microstructures

The actual chemical composition (wt%) of the 7050 alloy used for directional solidification is:

Cu	Si	Mg	Zn	Fe	Mn	Al
2.6	0.06	2.37	6.56	0.09	0.05	Bal.

This alloy was directionally solidified with the growth rate of 0.05, 0.1 and 0.2 mm/sec with a temperature gradient of 50 K/cm at liquid/solid interface. Figure 8 shows a typical microstructure of this alloy directionally solidified at a growth rate of 0.1 mm/sec. In addition to the (Al) phase, other precipitated phases include Mg_2Si, sigma, S-Al_2CuMg, θ-Al_2Cu, Al-Cu-Fe and Al-Fe-Mn-Si intermetallic compounds. These phases were identified using metallography and EPMA. Details of the phase identification will be presented in another paper.

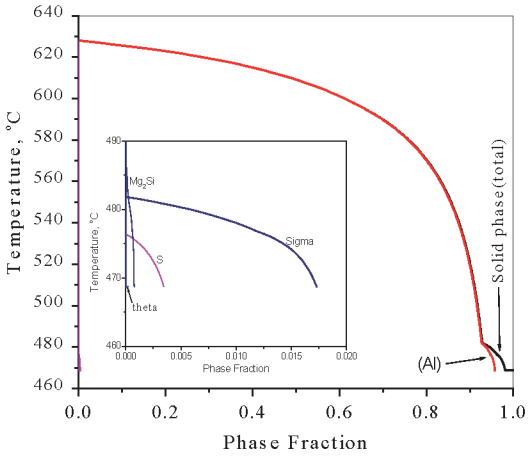

Figure 9 Model-calculated phase fraction for 7050 alloy showing the fractions of the phases present as a function of temperature with growth rate of 0.5mm/s; the insert shows an enlarged view for the temperature interval from 460 to 590°C

Figure 9 shows the predicted fractions of phases evolved during solidification for the 7050 alloy using the modified Scheil model. Fractions of Al-Cu-Fe and Al-Cu-Mn-Fe-Si intermetallic phases are very small and are not shown in Figure 9. Predicted fractions of (Al) for alloys solidified at three different growth rates are compared with the experimental data in Table III. The fraction of (Al) did not change much when the growth rate increased from 0.05 to 0.2 mm/sec. Predicted secondary dendrite arm spacing values are also compared with experimental measurements in Table III. Good agreement was obtained between the predicted values and measurements for this multi-component alloy.

Table III Comparison of experimental and calculated phase fractions and dendrite arm spacings

Growth Rate (mm/s)	λ_2,μm		Amount of Primary (Al), vol.%				
	Image Analysis	Model cal.	Area Scan	Image analysis	Model cal.	Scheil	Lever rule
0.05	67	68.1	92.7	94.7	94.7	89.0	98.3
0.1	56	55.2		94.8	94.8	89.0	98.3
0.2	42	44.1		95.0	94.8	89.0	98.3

It is worth noting that a knowledge on the evolution of phase fractions is valuable information for alloy design and process refinement. The amount of these intermetallic phases may have great influence on the properties of the final products. Normally, it is very difficult to experimentally determine the fractions of intermetallic phases, especially when too many phases are involved and the fraction of each phase is small. With this micromodel, these phase fractions can be predicted easily and accurately.

5.2.2 Microsegregation in directionally solidified 7050 alloys

The same method as used for Al-Cu-Mg-Si quaternary alloys was used to experimentally study the microsegregation in the 7050 alloy. A total of 767 measurements were automatically carried out over an area of 800X800μm^2 in transverse section of a 7050 alloy solidified at a growth rate of 0.05mm/sec. Figure 10 shows the measured concentrations for solute Cu, Mg, Zn, Fe, Mn and Si on 800X800 μm^2 area. Scientific graphing and analysis software ORIGIN 6.0 was used to create these concentration contour plots.

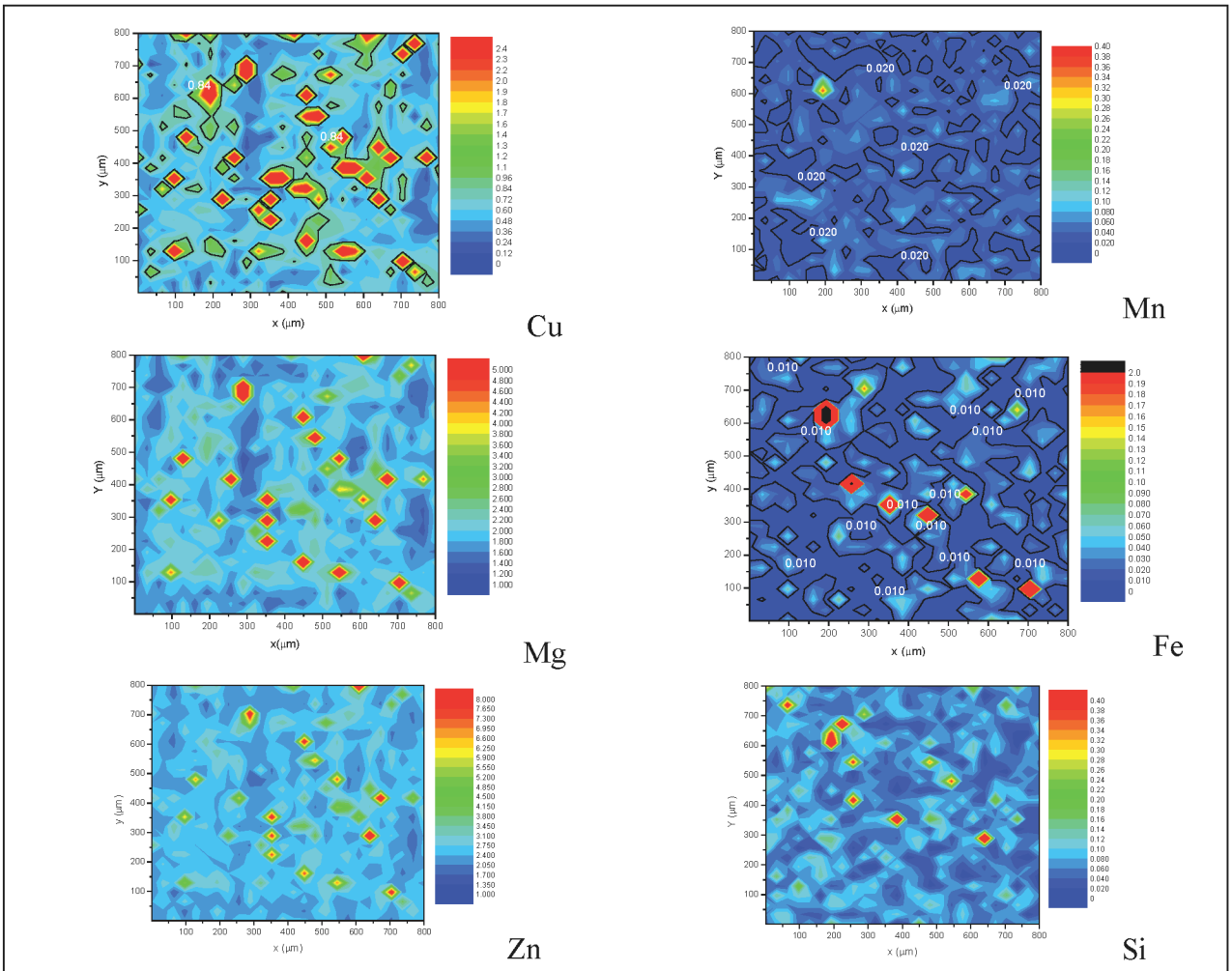

Figure 10. Experimentally determined solute concentration contour plots in directionally solidified 7050 alloy at a growth rate of 0.05mm/sec with temperature gradient of 50°C/cm

We first look the area with high Mn content in Figure 10-Mn. This area is also the high Fe, high Si and high Cu concentration area in Figure 10-Fe 10-Cu and 10-Si. But the Mg and Zn concentrations are not high in this area. This area corresponds with the formation of AlCuMnFeSi intermetallic phase. If we examine the high Zn areas in figure 10-Zn, we can always find the corresponding areas with high Mg and Cu contents in Figures 10-Mg and 10-Cu. These high Zn areas correspond with the formation of the σ-AlCuMgZn phase. Similarly, we can find the corresponding areas for Mg_2Si, AlCuFe and other phases. Figure 10 also shows clearly the concentration changes in the primary (Al) phase.

In order to obtain the composition vs fractions of solids profile for this alloy, the same approach as used previously for Al-Cu-Mg-Si quaternary alloy was applied. The measured solute distributions of Zn and Cu for a 7050 alloy solidified at growth rate of 0.05mm/s with temperature gradient of 50 K/cm are shown in Figures 11 and 12, respectively. Predicted results with the sphere model and under the Scheil conditions are also shown in Figure 11 and Figure 12 for comparison. Again, very good agreement was attained between experimental data and the prediction by the micro model. The results calculated by the Scheil model deviate significantly from the experimental data. Similar results were obtained for other solute components.

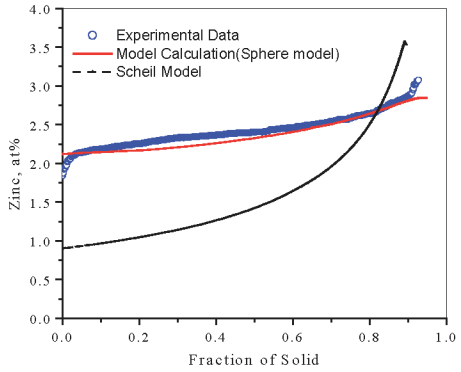

Figure 11. Zn concentration profiles in the primary dendrites as a function of the fraction of solid: comparison between the model-calculated values and experimental data for 7050 alloy solidified with a growth rate of 0.05 mm/s and a temperature gradient of 50°C/cm at the liquid /solid interface

6. Conclusions

A microscopic model has been directly coupled with multicomponent phase diagram calculation using the multicomponent phase diagram computation interface-PANDAT[15]. Back diffusion in solid during the solidification, dendrite arm coarsening and undercooling are considered in this micro-model.

Microsegregations in a quaternary Al-6.27Cu-0.22Si-0.19Mg(wt%) alloy and the 7050 commercial alloy have been investigated experimentally using directional solidification. A reliable EPMA area scan method was used for obtaining the solute distributions.

The predicted phase fractions and solute concentrations in primary (Al) using the present model are in very good agreement with the experimental data for both the quaternary and 7050 commercial alloys. The spherical model was found the best in approximating the shapes of the dendrite arms. The calculated values using the Scheil model always deviate significantly from the experimental data.

The 12-component Al database used in the present study was found to be reliable for these alloys. The micromodel, combining with the Al database, can be used as a powerful tool for the prediction of microstructure and microsegregation in multicomponent aluminium alloys under different cooling rates.

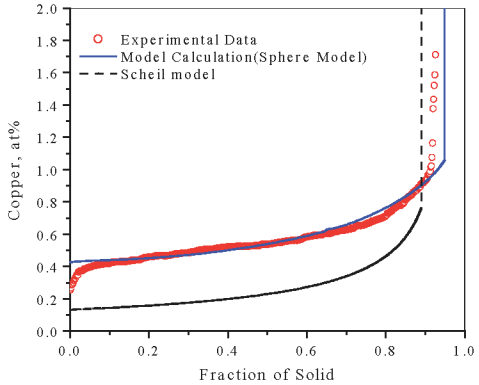

Figure 12. Cu concentration profiles in the primary dendrites as a function of the fraction of solid: comparison between the model-calculated values and experimental data for 7050 alloy solidified with a growth rate of 0.05 mm/s and a temperature gradient of 50°C/cm at the liquid /solid interface

Acknowledgement

We wish to thank the National Science Foundation for financial support through grant No. NSF-DMR-94-21780, and Dr. Bruce MacDonald of the Metal Program of the Materials and Processing Cluster of NSF for his interest. We also wish to thank the Air Force Laboratory, Dayton, OH, for the partial financial support through SBIR project (Nos. F33651-97-C-5257 and F33615-00-C5514) awarded to Computherm, LLC, Madison, WI 53719.

References

[1] W.J.Boettinger, S.R.Coriell, A.L.Greer, A.Krama, W.Kurz, M.Rappaz and R.Trivedi, *Acta mater.* 48, (2000), p43-70;
[2] R.Mehrabian and M.C.Flemings, *Metall. Trans.,* 1 (1970), pp455-464;
[3] T.Kraft and Y.A.Chang, *JOM,* Vol. 49, No.12 (1997),pp20-28;
[4] A. Roosz, E. Halder and H. E. Exner, *Mater. Sci. Tech.*, 1986, 2, 1149-1155.
[5] J. Lacaze and G. Lesoult, *ISIJ Int.*, 1995, 35, 658-664.
[6] A. Mortensen, *Metall. Trans. A*, 1989, 20A, 247-253.
[7] M. J. Aziz, *J. Appl. Phys.*1982, 53, 1158-68;
[8] M.J. Aziz and T. Kaplan, *Acta Metall.*, 1988, 36, 2335-47.
[9] M.J.Aziz and W.J.Boettinger, *Acta Metall. Mater.* 19994, 42, 527-37.
[10] A. Mortensen, *Metall. Trans. A*, 1989, 20A, 247-253.
[11] T. Kraft, M. Rettenmayr and H. E. Exner, *Model. Simul. Mater. Sci. Eng.*, 1996, 4, 161-177.
[12] Xinyan Yan, Fanyou Xie, M. Chu and Y. A. Chang, Mater. Sci. Eng. A, 2000, at press.
[13] L. Kaufman and H. Bernstein, *Computer Calculation of Phase Diagrams,* Academic Press, New York, 1970.
[14] F-Y. Xie, Ph.D Thesis, University of Wisconsin-Madison, 1999.
[15] PANDAT 1.0-Phase Diagram Calculation Engine for Multicomponent Systems, Computherm LLC, 437 S. Yellowstone Dr., Suite 217, Madison, WI53719, 2000.
[16] R. C. Beaverstock, in "*Solidification Processing 1997*", eds. J. Beech and H. Jones, Dept. Engr. Mater., University of Sheffield, Sheffield, UK, 1997, p321-324.
[17] D.A. D.A. Petrov, N.D. Nagorskaya, Zhurnal Obshchei Khimii, 1949, 19, 1994-2037.
[18] L.F.Modolfo, Aluminium Alloys:Structure and Properties, London, 1976.
[19] Jacques Lacaze, Gerard Lesoult, Olivier Relave, Ibrahim Ansara, and Jean Pierre Riquet, Z.Metallk. , 78, 2, 1987, 141-150.
[20] D.J. Chakrabarti and J.L. Murray, Materials Science Forum, 1996, 217-222.
[21] H.W.L.Phillips, Aluminium Devel. Ass., London, Inf. Bull. 25, 1961
[22] F. Zhang et al., CompuTherm, LLC, 437 S. Yellowstone Dr., Suite 217, Madison, WI 53719, USA, 2000.
[23] Xinyan Yan, Y.A.Chang, University of Wisconsin-Madison, Madison, WI53706, 2000, unpublished results.
[24] H. Liang, Ph.D Thesis, University of Wisconsin-Madison, 1998.